Water Air Soil Pollut (2018) 229: 67
https://doi.org/10.1007/s11270-018-3728-y

Highly Efficient Cuprous Oxide Nanocrystals Assisted with Graphene for Decolorization Using Visible Light

Shou-Heng Liu · Sheng-Wei Yang

Received: 16 October 2017 / Accepted: 30 January 2018 / Published online: 14 February 2018

Abstract The preparation of rhombic dodecahedral cuprous oxide (rdCu_2O) decorated with various amounts of reduced graphene oxide (rGO) is carried out by using a wet-chemical route. The resultant nanocomposites (denoted as rdCu_2O-*x*rGO, *x* = amounts of rGO) possess unique crystal facets of Cu_2O and superior electronic properties of rGO, which are tested as photocatalysts in the degradation of methyl orange (MO) under visible light irradiation. Among all the rdCu_2O-*x*rGO photocatalysts, the rdCu_2O-1rGO is found to degrade ca. 98% of MO in the presence of very low catalyst concentration (0.0625 g L^{-1}) within 120 min under visible light illumination. This obtained result may be owing to the well interfacial contact of rhombic dodecahedral Cu_2O nanoparticles with high electronic conductivity of rGO sheets that can increase the separation of photo-induced electron-hole pairs, stabilize the Cu_2O, and enhance MO adsorption, which are proofed by using X-ray diffraction, scanning electron microscopy, X-ray photoelectron spectroscopy, photoluminescence, and UV-Vis diffuse reflection spectroscopy. Most importantly, these efficient photocatalysts can be reusable and retain surpassing photoactivity in terms of MO degradation after cyclic tests, which may provide a possible opportunity for practical applications in purifying wastewater via direct sunlight.

S.-H. Liu (✉) · S.-W. Yang
Department of Environmental Engineering, National Cheng Kung University, Tainan 70101, Taiwan
e-mail: shliu@mail.ncku.edu.tw

Keywords Cuprous oxide · Nanocrystal · Reduced graphene oxide · Visible-light-sensitive · Durability

1 Introduction

Synthetic dyes, hazardous and dangerous to the natural environment, are intensively used in textile, cosmetic, paper, leather, pharmaceutical, and food manufacturing. In particular, great amounts of dye wastewater from textile factories which cannot be degraded easily are released into the aquatic surroundings. Photocatalysis has been significantly investigated for the treatments of environmental-related pollution, e.g., hazardous air and organic-polluted wastewater (Gonzalez et al. 2017; Granbohm et al. 2017). Among all photocatalysts, the metal oxide semiconductors have been demonstrated to exhibit superior UV-light photocatalytic performance. Nevertheless, very less solar energy with UV wavelength (< 10%) in the direct sunlight can be applied, resulting in the obstacles of their practical applications in the real industrials (Liu and Syu 2012; Liu and Syu 2013; Liu et al. 2014; Landi et al. 2017; Leon et al. 2017). Recently, research works have been widely dedicated to enhancing their photocatalytic activities by improving the visible-light-responsive (ca. 43% of visible light in the solar spectrum) ability of prepared photocatalysts and decreasing the recombination of the photogenerated electrons and holes as well. To achieve the goal, several possible methods have been proposed by using the routes including doping the photocatalysts with non-metal ions and/or metal ions (Altin and

Sokmen 2014; Tangale et al. 2014; Nalbandian et al. 2015; Choi et al. 2016; Kumar and Ojha 2016; Bailón-García et al. 2017), decoration of carbon nanomaterials onto photocatalysts (Liu et al. 2016a; Su et al. 2016; El-Sheikh et al. 2017), dye/surface complex sensitization (Reddy et al. 2016; Chowdhury et al. 2017; Yu et al. 2017), and coupling two or more semiconductors (Nadarajan et al. 2016; Petronella et al. 2017). Accordingly, the modified photocatalysts via aforementioned methods exhibit the surpassing separation of electron-hole pairs, resulting in the remarkable advance in the visible-light-responsive activity.

Among various semiconductors, cuprous oxides (Cu_2O) have been extensively studied in the fields of photocatalytic reactions because of their abundance, low toxicity (Wang et al. 2002; Chen et al. 2012; Kwon et al. 2015; Kumar et al. 2016; Mateo et al. 2017), and superior visible-light response (bandgap energy = ca. 2.0 eV). Moreover, the improvement on the photocatalytic oxidation of organic dyes by crystal structure of Cu2O via visible light illumination has been investigated (Huang et al. 2012; Shang and Guo 2015; Yeo et al. 2017). However, the photocatalytic activities of these Cu_2O nanocrystals are still restricted due to the recombination of the photo-induced electron-hole pairs (Tao et al. 2017) and poor durability (Sun 2015) during the photocatalysis. Therefore, several works (Babu et al. 2015; Shen et al. 2015; Liu et al. 2016b) have been done by the incorporation of carbon materials onto Cu_2O in order to circumvent the aforementioned issues. Among various nanocarbons, graphene/reduced graphene oxide exhibits the two-dimensional (2D) sp^2-bonded carbon structure (Bajpai et al. 2017) with unique properties (surpassing electron mobility of 2×10^5 cm^2 V^{-1} s^{-1} (Mayorov et al. 2011), high theoretical surface area of ca. 2965 m^2 g^{-1} (Stoller et al. 2008), and remarkable thermal and chemical stability) (Tan et al. 2015; Khurana et al. 2017; Ojha et al. 2017) which render graphene a promising support for photocatalytic applications. As such, the preparation of Cu_2O-graphene composites, which can possess highly visible-light-responsive performance in the applications of organic pollutants remediation and fuel production, was reported (Li et al. 2016; Liu et al. 2016a; Zou et al. 2016).

In this study, the Cu_2O crystals with {110} facets decorated with different amounts of graphene sheets (denoted as rdCu_2O-*x*rGO, *x* = amounts of rGO) were prepared by using a facile wet-chemical method. These rdCu_2O-*x*rGO samples were systematically identified by a series of analytical techniques. Additionally, they were also used as photocatalysts in the decolorization of methyl orange (MO) under visible light. As a result, the Cu_2O rhombic dodecahedra decorated with 1 wt% of graphene sheets demonstrate the best photocatalytic activity of MO degradation while compared to the other rdCu_2O-*x*rGO. More importantly, the stability of the rdCu_2O-1rGO composites is notably superior to that of pure Cu_2O crystals.

2 Experimental

2.1 Preparation of GO

Graphene oxide (GO) was synthesized via a modified route in the previous report (Nethravathi and Rajamathi 2008) and described as below. After adding 6 g of graphite and 3 g of $NaNO_3$ into 150 mL of concentrated H_2SO_4 under stirring at 273 K, 18 g of $KMnO_4$ was slowly introduced and stirring constantly at 308 K for 45 min. Then, 276 mL of deionized (DI) water was mixed with the above solution and then stirred continuously for 60 min. After that, 60 mL of 30% H_2O_2 and 840 mL of DI water were added to the resultant solution. Finally, the resulting solids were washed several times with 5% of HCl and dried at 333 K.

2.2 Preparation of Rhombic Dodecahedral Cu_2O-Graphene

About 138 mL of deionized water with different amounts of GO (0.5, 1, 2, 10, and 20%) was stirred at 307 K. After dissolving ca. 10 mL of 0.1 M $CuCl_2$ solution and 1.7 g of sodium dodecyl sulfate (SDS) solids in above solution, 10 mL of 1.0 M sodium hydroxide (NaOH) solution and 48 mL of 0.1 M hydroxylamine hydrochloride were introduced and stirred at 298 K for 1 h. Lastly, the resulting solids were centrifuged, washed with water/ethanol mixture, and then dried under vacuum. The obtained photocatalysts in this study were denoted as 12-G (*x*%), where *x* represents the amounts of graphene.

2.3 Photocatalytic Degradation

First, 5.0 mg of photocatalysts were well suspended in 80 mL of 15 mg L^{-1} MO aqueous solution using ultrasonic treatments. Then, the aqueous solution was kept stirring in the dark for 2 h to achieve the adsorption equilibrium. Photodegradation experiments of MO were carried out at 298 K in a Pyrex reactor (100 mL)

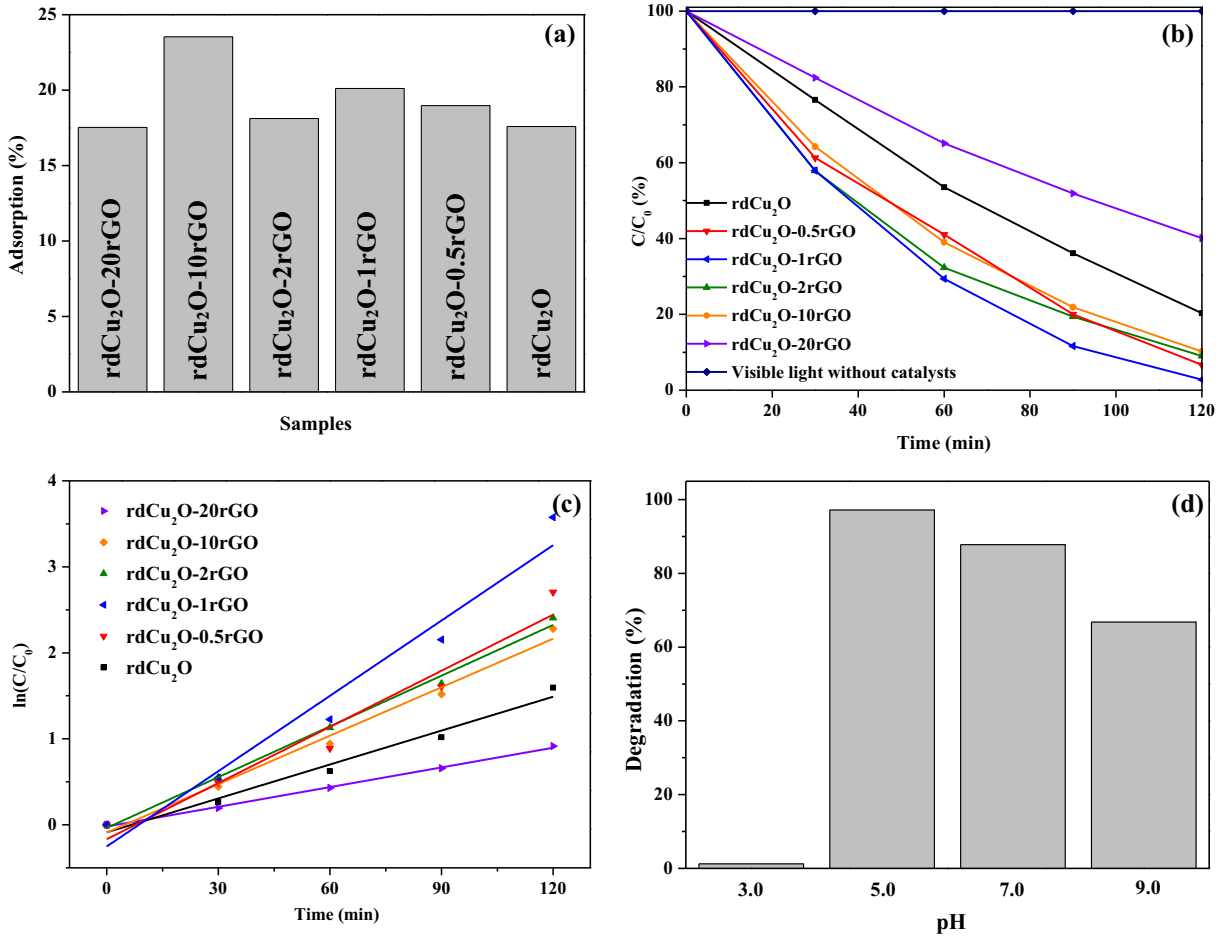

Fig. 1 **a** MO adsorption capacities of various photocatalysts. **b** Visible-light-driven photodegradation of MO on the photocatalysts, **c** their respective kinetic plots obtained from (**b**) data, and **d** pH effect on photodegradation of MO by rdCu2O-1rGO

equipped with a water-circulation cooling system. The solution was irradiated by a 300 W Xe lamp (Newport, Model 66142) with a 420 nm cut-off filter to remove UV contribution. For each time interval (30 min), about 2 mL of suspension was repeatedly withdrawn and filtered to record the concentration changes by using a UV-Vis spectrophotometer (Hitachi, U-2910). Reproducibility was determined by repeating the photocatalytic tests at least three times. The data can be acquired with a relative standard deviation within 5%.

2.4 Characterizations of Photocatalysts

The crystalline structures of all samples were identified by an X-ray diffractometer (XRD, PANalytical X'Pert PRO) with a Cu Kα radiation ($\lambda = 1.541$ Å). The particle size and morphologies of the photocatalysts was studied by a field-emission scanning electron microscope (SEM, JEOL JSM-7000F) operated at accelerating voltages of 20 kV. X-ray photoelectron spectroscopy (XPS) analysis of samples was performed by using a Kratos AXIS Ultra DLD spectrometer system with a monochromatic Al Kα X-ray source (1486 eV). Binding energies of the photoelectrons were referenced relative to adventitious carbon at 284.6 eV. The photoluminescence (PL) emission spectra were measured by using a fluorescence spectrophotometer (Horiba Jobin Yvon LabRAM HR) at an excitation wavelength of 325 nm. The UV-Vis diffuse reflection spectra of the samples in the wavelength of 400–800 nm were attained on a UV-Vis spectrophotometer (Varian, Cary 100).

3 Results and Discussion

The photocatalytic performance of $rdCu_2O$ and various $rdCu_2O$-*x*rGO nanocomposites were examined

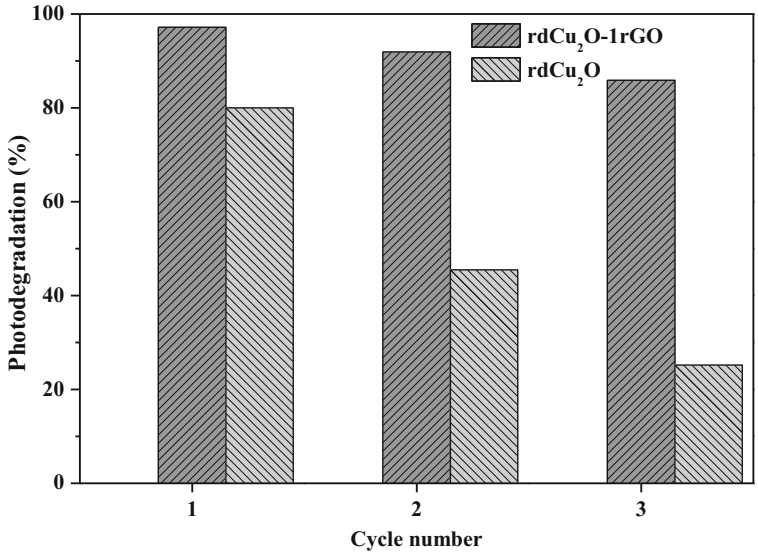

Fig. 2 Cyclic tests of $rdCu_2O$ and $rdCu_2O$-1rGO photocatalysts for three cycles of visible-light photodegradation of MO

via the photodegradation of the MO solution (pH = 5) under visible light irradiation at room temperature. As shown in Fig. 1a, the adsorption capacities of MO on $rdCu_2O$, $rdCu_2O$-0.5rGO, $rdCu_2O$-1rGO, $rdCu_2O$-2rGO, $rdCu_2O$-10rGO, and $rdCu_2O$-20rGO after 120 min in dark are 17.6, 19.0, 20.1, 18.1, 23.5, and 17.5%, respectively, suggesting that the existence of reduced graphene oxide (rGO) could enhance the adsorption of MO molecules. It should be noted that the decreased adsorption of MO observed for $rdCu_2O$-20rGO may be due to the fact that excessive amounts of rGO result in the aggregation. The concentration variations (C/C_0, where C_0 is the concentration after equilibrium in 120 min) of MO versus irradiation time are displayed in Fig. 1b. The photocatalytic degradation of MO for the $rdCu_2O$ photocatalysts was found to be greatly enhanced (ca. 80% of MO degradation) while compared to the result without catalysts under visible light. Upon incorporating rGO (0.5–10 wt%) onto $rdCu_2O$, the photodegradation of MO can be further improved, suggesting that the existence of rGO can enhance the photocatalytic efficiency. However, the photoactivity of $rdCu_2O$-20rGO was observed to be worse than that of pristine $rdCu_2O$. This finding may be ascribed to the excessive rGO which can create the recombination centers to hinder charge separation, as reported earlier (Pu et al. 2017). In addition, more rGO could result in the deterioration of crystallization (discussed later in the XRD and SEM results) in

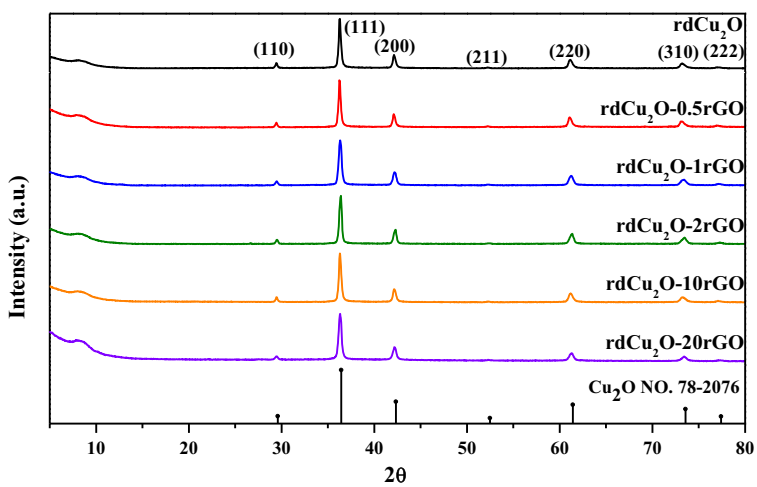

Fig. 3 Powdered XRD patterns of $rdCu_2O$ and various $rdCu_2O$-*x*rGO photocatalysts

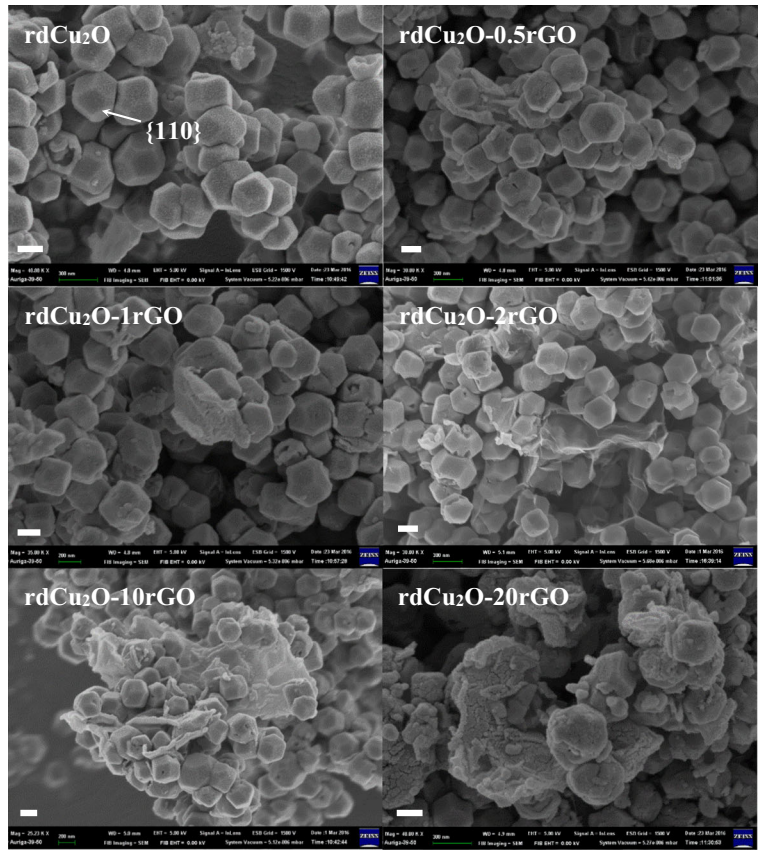

Fig. 4 SEM images of $rdCu_2O$ and various $rdCu_2O$-*x*rGO photocatalysts (the scale bar = 200 nm)

the $rdCu_2O$-*x*rGO photocatalysts. Among all the prepared photocatalysts, ca. 98% of MO can be photodecomposed by $rdCu_2O$-1rGO in 120 min under visible light illumination. This result could be attributed to the fact that excited electrons on the $rdCu_2O$ could rapidly transfer to the high conductivity of suitable amounts of rGO sheets without electron-hole recombinations (Huang et al. 2017a; Huang et al. 2017b; Kecsenovity et al. 2017). Excessive amounts of rGO can inhibit the growth of crystal facets (mentioned below) and create recombination centers as well in the $rdCu_2O$-*x*rGO photocatalysts. It is worthy to note that the potential of conduction band for Cu_2O is − 3.0 eV vs. vacuum (Gao et al. 2012) which is higher than that of LUMO for MO (− 3.3 eV vs. vacuum) (Chang et al. 2012). Consequently, the electron transfer from the excited MO toward Cu_2O could barely happen, implying the probability of MO sensitization can be excluded. As shown in Fig. 1c, the pseudo-first-order reaction observed for $rdCu_2O$ and various $rdCu_2O$-*x*rGO photocatalysts and their corresponding rate constant (k) of degradation kinetics can be obtained. Accordingly, the k values of the $rdCu_2O$, $rdCu_2O$-0.5rGO, $rdCu_2O$-1rGO, $rdCu_2O$-2rGO, $rdCu_2O$-10rGO, and $rdCu_2O$-20rGO photocatalysts are ca. 0.013, 0.022, 0.029, 0.020, 0.019, and 0.008 min^{-1}, respectively. This result confirms that $rdCu_2O$-1rGO photocatalyts possess the best activity among the prepared samples. In addition, since the pH of MO solution may have strong impact on photodegradation, the effect of initial pH on MO photodegradation by the $rdCu_2O$-1rGO was also investigated and shown in Fig. 1d. It can be seen that the photodegradation efficiency of MO is significantly depending on the pH value of solution, which follows the order under different pH value: pH (5.0) > pH (7.0) > pH (9.0) > pH (3.0). Under the alkali condition (pH = 9.0), the photodegradation efficiency of MO solution is relatively low (the degradation efficiency in 120 min is ca. 66.8%), which may be due to the formation of surface hydroxyl groups ($–O^-$) in the $rdCu_2O$-1rGO nanocomposites. This would decrease the adsorption affinity of MO onto the catalyst surface. In addition,

the possible dissolution of Cu ions from the $rdCu_2O$-1rGO nanocomposites to solution under strong acidic condition (pH = 3.0) may happen (Feng et al. 1997).

It is important to investigate the durability and reusability in order to evaluate the practical applications of the photocatalysts. Herein, the $rdCu_2O$ and $rdCu_2O$-1rGO are taken as the representative samples to examine their stability of MO photodegradation. As shown in Fig. 2, an evident decline (i.e., from 80.0 to 25.2%) of photocatalytic degradation efficiency is observed for $rdCu_2O$ photocatalysts after three continuous runs. Nonetheless, only ca. 11% of efficiency loss, which may be attributed to the occurrence of intermediates (Liu et al. 2011) during photodegradation process, is found for $rdCu_2O$-1rGO. The enhanced durability is clearly due to the incorporation of graphene onto the $rdCu_2O$ photocatalysts.

In order to realize the influence of rGO on the physicochemical properties of $rdCu_2O$ photocatalysts, various spectroscopic analyses were carried out. As can be seen in Fig. 3, seven diffraction features at $2\theta = 29.6°$, 36.4°, 42.3°, 52.5°, 61.4°, 73.6°, and 77.5° in the XRD patterns of synthesized photocatalysts are respectively indexed to the (110), (111), (200), (211), (220), (311), and (222) crystal planes of pure Cu_2O. It is noteworthy that no metallic and oxidized copper (i.e., CuO) can be observed in the XRD patterns, suggesting the almost total reduction of Cu(II) precursors to Cu_2O by NH_2OH. According to the previous report (Huang et al. 2012), rhombic dodecahedral Cu_2O has the intensity ratio of the (220) peak to the (200) peak (i.e., $I_{(220)}/I_{(200)}$) of ca. 0.79. In this study, the value of $I_{(220)}/I_{(200)}$ observed for $rdCu_2O$ is 0.79, indicating the formation of rhombic dodecahedral structure. While incorporating small amounts of rGO (0.5–1.0 wt%) onto $rdCu_2O$ ($rdCu_2O$-0.5rGO and $rdCu_2O$-1rGO), the $I_{(220)}/I_{(200)}$ values are almost the same as that of pristine $rdCu_2O$. However, upon gradually decorating more rGO onto rhombic dodecahedral Cu_2O ($rdCu_2O$-*x*rGO, $x = 2$–20), the intensity ratio of $I_{(220)}/I_{(200)}$ is decreased (from 0.79 to 0.67), suggesting that the distortion of crystal structure may occur.

The crystal structures of these Cu_2O nanocrystals were further studied by SEM images. As shown in Fig. 4, the pristine Cu_2O exhibits rhombic dodecahedral structure (mainly {110} facets) with average particle size of ca. 300–500 nm. The thin layers of rGO are decorated onto the $rdCu_2O$ nanocrystals in the $rdCu_2O$-*x*rGO photocatalysts ($x = 0.5$–20). In addition, the averaged particle sizes of all $rdCu_2O$-*x*rGO photocatalysts are almost unchanged. However, it

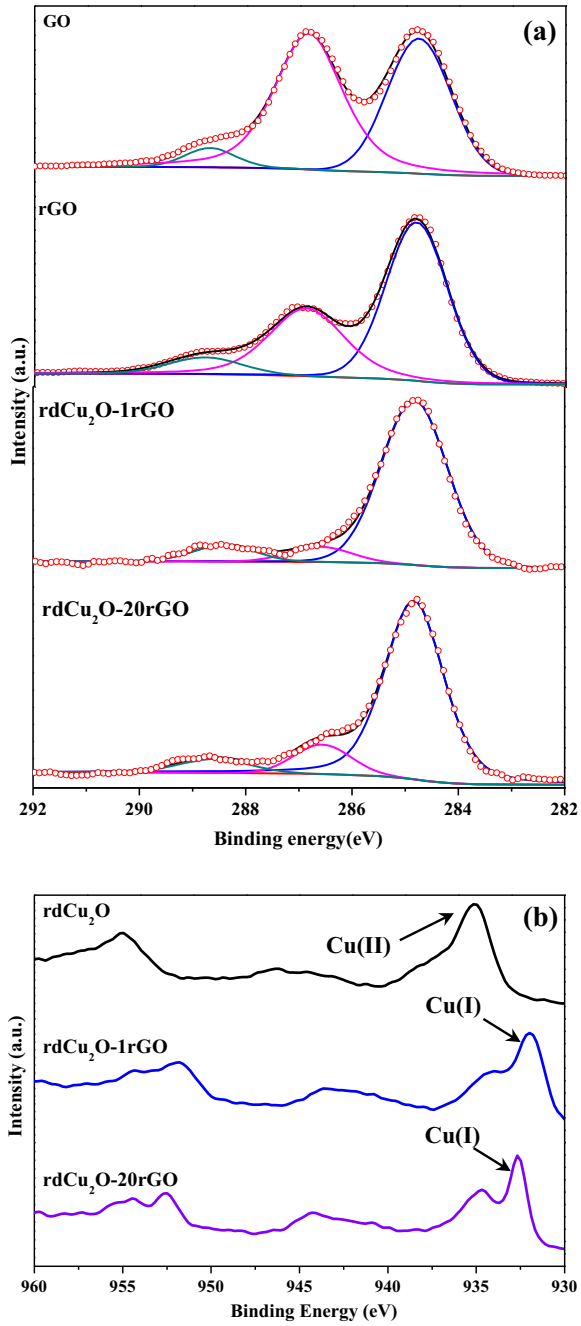

Fig. 5 XPS spectra of various photocatalysts at the **a** C 1 s and **b** Cu 2p regions

appears that the rhombic dodecahedral structures of $rdCu_2O$-20rGO photocatalysts are destroyed upon incorporating 20 wt% of rGO, suggesting that the excessive rGO may inhibit the crystallization process of $rdCu_2O$ nanocrystals. This finding is in good agreement with the aforementioned XRD result.

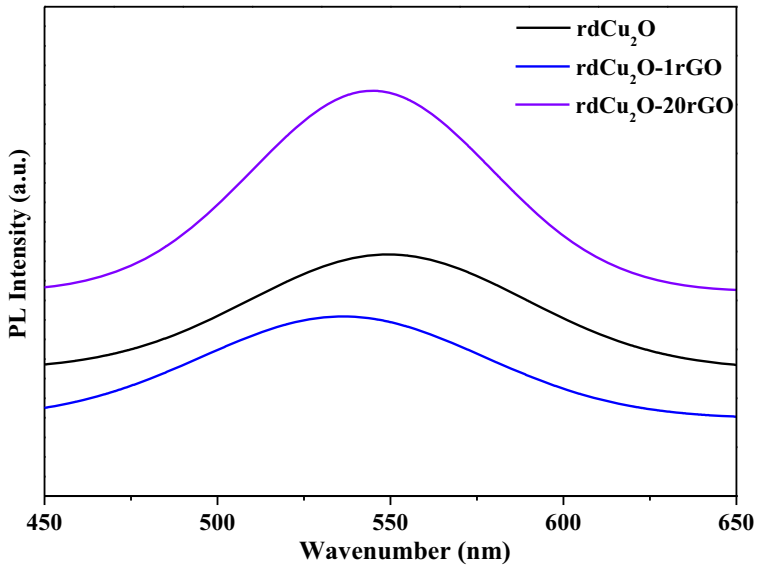

Fig. 6 PLspectra of $rdCu_2O$, $rdCu_2O$-1rGO, and $rdCu_2O$-20rGO photocatalysts

In order to study the chemical compositions of various photocatalysts, the X-ray photoelectron spectra (XPS) were further collected and displayed in Fig. 5. The magnified XPS spectra in the C1s region (see Fig. 5a) show three peaks at 284.6, 286.5, and 288.4 eV, which can be attributed to sp^2-hybridized (C=C), epoxy/hydroxyl (C-O) and carboxyl (C=O) carbons, respectively (Stankovich et al. 2007; Zhang et al. 2010). It can be seen that the intensities of the peaks at 286.5 and 288.4 eV in the rGO and rCu_2O-*x*rGO ($x = 1$ and 20) photocatalysts are decreased obviously as compared to that of GO, indicating that the majority of GO is transformed to rGO. In addition, the Cu2p XPS spectra (see Fig. 5b) of the prepared photocatalysts show the primary peak with binding energy of ca. 934 eV and satellite feature of ca. 945 eV, which are assigned to Cu(II). However, the peak at ca. 932 eV is ascribed to Cu(I) species (Wang et al. 2002). It should be noted that the amounts of Cu(II) species observed for $rdCu_2O$-1rGO and $rdCu_2O$-1rGO photocatalysts are much less than that of $rdCu_2O$, implying that rGO sheets can stabilize Cu(I) species in the composites. The stabilization of active Cu_2O nanocrystals could play a critical role in the long-term photodegradation process (Pu et al. 2017). As mentioned in the previous XRD data (see Fig. 3), no diffraction peaks of CuO can be observed. This result can be explained that the crystal structure of the prepared photocatalysts is identified in the bulk phase via XRD. Nonetheless, XPS could provide the information of surface structure (< 5 nm) only for several atomic layers. Therefore, it is difficult to obtain the bulk information of copper in the photocatalysts.

The interface charge transfer and the recombination rate of photoexcited electron-hole pairs are further explored by photoluminescence (PL) spectra (Haldar et al. 2012). Generally, the relative intensities of peaks in PL spectra can be correlated with photoexcited charge carrier lifetimes (Das and De 2009). As displayed in Fig. 6, a broad peak located in the range of 450 to 650 nm can be found due to the electron transition from the conduction band to the Cu d-level of the valence band (Dahl and Switendick 1966). It is worthy to note that the $rdCu_2O$-1rGO photocatalysts possess the much lower peak intensity than $rdCu_2O$, indicating that the decoration of 1 wt% of rGO onto $rdCu_2O$ can lead to the reduced possibility of recombination in the electron-hole pairs. This finding is possibly due to the well interfacial contact between rGO and crystal facets of rhombic dodecahedral Cu_2O, which matches well with the earlier reports (Niu 2014). However, the PL intensity of $rdCu_2O$-20rGO nanocomposites is found to be higher than that of $rdCu_2O$-1rGO and $rdCu_2O$, implying that the recombination rate of photogenerated electrons-holes in the $rdCu_2O$-20rGO photocatalysts is noticeably increased in the presence of 20 wt% of rGO.

The effects of rGO on the photoresponse of the $rdCu_2O$-*x*rGO photocatalysts were explored by UV-Vis absorption spectroscopy. As can be seen in Fig. 7, a band-gap absorption edge at ca. 590 nm in visible region can be observed for $rdCu_2O$. This suggests that $rdCu_2O$ exhibits the intrinsic bandgap of ca. 2.2 eV which is a

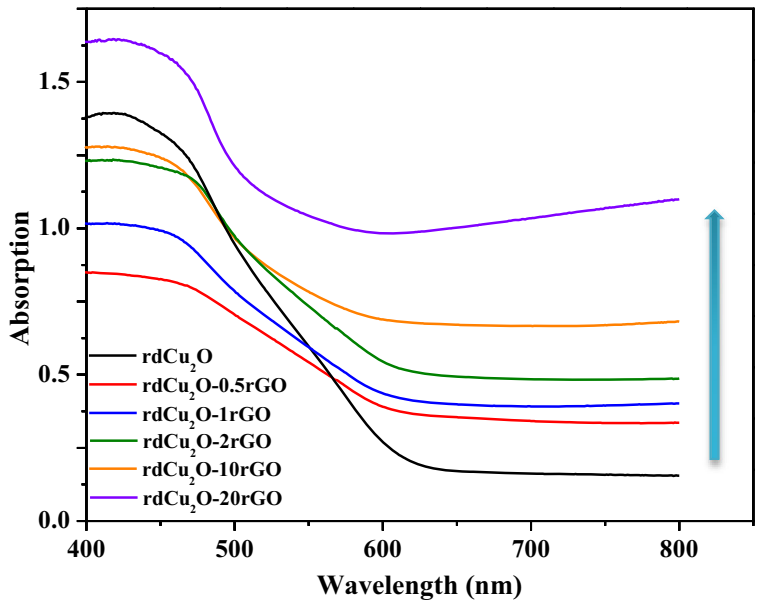

Fig. 7 UV-Vis spectra of $rdCu_2O$ and various $rdCu_2O$-*x*rGO photcatalysts

visible-light-reactive semiconductor. Moreover, various $rdCu_2O$-*x*rGO photocatalysts demonstrate higher absorbance in the entire visible-light region upon the gradual incorporation of rGO onto $rdCu_2O$. This finding proves that the $rdCu_2O$-*x*rGO nanocomposites can improve the absorbance of solar sunlight. Based on the combined data of the XRD, SEM, XPS, PL, and UV-Vis spectra, the $rdCu_2O$-*x*rGO photocatalysts possess rhombic dodecahedral Cu_2O incorporated with 1 wt% of rGO nanosheets which can decrease the recombination of electron-hole pairs, making better use of solar energy for decolorization of wastewater.

From the integrative results, a possible mechanism of the photodegradation of MO by $rdCu_2O$-*x*rGO is proposed. Upon visible light irradiation, the rhombic dodecahedral Cu_2O absorb incident photons to generate electrons

Table 1 Comparison of photocatalytic performance of different Cu_2O-based composites for degradation of dyes

Catalysts	Morphology	$C_{catalyst}$[a] (g L^{-1})	C_{dye}[b] (mg L^{-1})	T[c] (min)	η[d] (%)	Light source	Reference
Cu_2O/rGO aerogel	NP[e]	1.00	MO (5)	300	70	Visible	Cai et al. 2015
Cu_2O@3D-rGO	NP[e]	0.20	RhB (5)	150	95	Daylight	Zhang et al. 2016b
Ag-Cu_2O/rGO	NP[e]	0.20	MO (40)	60	87	Visible	Xu et al. 2015
Cu_2O/carbon	NP[e]	0.50	MO (20)	120	55	Daylight	Zhou et al. 2013
Cu_2O/ZnO	NP[e]	1.00	MO (25)	180	75	Visible	Xu et al. 2010
Cu_2O/PA/rGO	Cubic	0.50	MO (30)	180	95	Visible	Wang et al. 2013
Cu_2O-rGO	Cubic	0.40	MO (15)	100	~100	Visible	Zhang et al. 2016a
Cu_2O/$BiVO_4$	Polygonal	1.25	MO (5)	120	76	Visible	Li et al. 2014
Cu_2O-rGO	Octahedra	0.33	MB (10)	120	72	Visible	Zou et al. 2016
$rdCu_2O$-1rGO	Rhombic dodecahedra	0.06	MO (15)	120	98	Visible	This work

[a] Catalyst concentration

[b] Different dye and their initial concentration

[c] Reaction time

[d] Removal efficiency

[e] Nanoparticle

and holes in the conduction band (CB) and valence band (VB) (Eq. (1)), respectively. Afterwards, the excited electrons quickly transfer from CB of rdCu_2O-*x*rGO to the rGO nanosheets (lower Fermi level = 0 V vs. NHE) which are possibly due to the stronger interaction between unique crystal facets and superior electrical conductivity of rGO (Eq. (2)). Then, the electrons adsorbed on rGO can react with the dissolved oxygen (O_2) to produce reactive oxygen peroxide radicals ($\bullet O_2^-$) (Eq. (3)) because the difference between reduction potential of $O_2/\bullet O_2^-$ (− 0.16 V vs. NHE) and Fermi level potential of rGO (ca. 0 V vs. NHE) (Wang et al. 2014) is insignificant. As a result, electron-hole recombination rate can be reduced. The generated $\bullet O_2^-$ may be transformed to HOO• which could react with the electrons to produce H_2O_2, and eventually to generate OH• radicals (Eq. (4)–(6)) (Wu et al. 1998). Nevertheless, positive charged holes (h^+) generated on the VB of rdCu_2O would not react with OH^- from absorbed water to generate surface hydroxyl radicals (•OH) since the VB potential of Cu_2O (+ 0.6 V vs. NHE) is lower than that of producing •OH radicals (+ 2.9 V vs. NHE) (Zou et al. 2016). Accordingly, the superoxide radical anions and further generating hydroxyl radicals may be the principal species for degrading MO into CO_2, H_2O, and intermediates under visible light (without dye sensitization) (Pu et al. 2017).

$$\text{rdCu}_2\text{O} + \text{hv} \rightarrow \text{rdCu}_2\text{O}(e^- + h^+) \quad (1)$$

$$e^- + \text{rGO} \rightarrow \text{rGO}\ (e^-) \quad (2)$$

$$\text{rGO}\ (e^-) + O_2 \rightarrow \text{rGO} + \bullet O_2^- \quad (3)$$

$$\bullet O_2^- + H^+ \rightarrow \text{HOO}\bullet \quad (4)$$

$$\text{HOO}\bullet + e^- + H^+ \rightarrow H_2O_2 \quad (5)$$

$$H_2O_2 + e^- + \rightarrow \bullet\text{OH} + OH^- \quad (6)$$

$$\bullet\text{OH} + \text{MO} \rightarrow \text{intermediates} + CO_2 + H_2O$$

It is noteworthy that our prepared photocatalysts exhibit the superior kinetic photodegradation rate of dye (removal efficiency = ca. 98% in 120 min) by using very low concentration of photocatalysts (0.0625 g L^{-1}) under visible light. Furthermore, the rdCu_2O-*x*rGO photocatalysts are not only fabricated via a simple wet-chemical method but also low in cost. As we know, the treatment of textile wastewater is carried out by several methods, including physical, chemical, and biological routes. In general, physical (e.g., membrane filtration) and advanced oxidation process (e.g., ozonation and Fenton oxidation) are effective for the degradation of dye in textile wastewater when the volume of textile effluent is small. Moreover, the cost of above-mentioned technologies is relatively high, which limits their large-scale applications. Compared to biological treatments, the photodecomposition of MO by prepared photocatalysts was found to possess the highly kinetic photodegradation rate (removal efficiency = ca. 98% in 120 min) via using very low concentration of photocatalysts (0.0625 g L^{-1}) under visible light. As compared to other Cu_2O-based photocatalysts reported in the earlier works (see Table 1), the rdCu_2O-1rGO with surpassing visible-light-active photocatalytic properties can be more efficient to make the potential application of direct sunlight utilization for treatment of organic pollutants in wastewater.

4 Conclusions

In this work, the rhombic dodecahedral Cu_2O photocatalysts decorated with different amounts of rGO are synthesized by using a facile wet-chemical method. Among all the photocatalysts, the obtained results show that the rdCu_2O-1rGO (1 wt% of rGO incorporation) photocatalysts have the best photocatalytic activity, namely, using very low concentration of photocatalysts (0.0625 g L^{-1}) to attain ca. 98% photodegradation of MO under visible-light irradiation within 120 min, which is also comparable to the earlier reported Cu_2O-based photocatalysts. The notable improvement in the photocatalytic performance may be attributed to the distinctive interfacial contact of rhombic dodecahedral Cu_2O nanoparticles with the surface of rGO nanosheets. The high electrical conductivity of rGO can promote the overall separation ability of photogenerated electron-hole pairs (evidenced by PL), stabilize the Cu_2O (identified by XPS), and enhance adsorption amounts of MO. As a result, the superior visible-light-sensitive photocatalytic properties (activity and durability) of rdCu_2O-*x*rGO photocatalysts render a

promising candidate for industrial applications in the wastewater treatments by employing solar energy.

Acknowledgements Financial supports of this work from the Ministry of Science and Technology of Taiwan (Contract No.: MOST 104-2628-E-006-018-MY3) are gratefully acknowledged.

References

Altin, I., & Sokmen, M. (2014). Photocatalytic properties of silver incorporated titania nanoparticles immobilized on waste-derived polystyrene. *Water, Air, and Soil Pollution, 225*(1), 1786.

Babu, S. G., Vinoth, R., Narayana, P. S., Bahnemann, D., & Neppolian, B. S. (2015). Reduced graphene oxide wrapped Cu_2O supported on C_3N_4: an efficient visible light responsive semiconductor photocatalyst. *APL Materials, 3*(10), 104415.

Bailón-García, E., Elmouwahidi, A., Álvarez, M. A., Carrasco-Marín, F., Pérez-Cadenas, A. F., & Maldonado-Hóda, F. L. (2017). New carbon xerogel-TiO_2 composites with high performance as visible-light photocatalysts for dye mineralization. *Applied Catalysis B Environmental, 201*, 29−40.

Bajpai, A. K., Dubey, R., & Bajpai, J. (2017). Synthesis, characterization, and adsorption properties of a graphene composite sand (GCS) and its application in remediation of Hg(II) ions. *Water, Air, and Soil Pollution, 228*(9), 346.

Cai, J. Y., Liu, W. J., & Li, Z. H. (2015). One-pot self-assembly of Cu_2O/RGO composite aerogel for aqueous photocatalysis, one-pot self-assembly of Cu_2O/RGO composite aerogel for aqueous photocatalysis. *Applied Surface Science, 358*, 146–151.

Chang, X., Gondal, M. A., Al-Saadi, A. A., Ali, M. A., Shen, H., Zhou, Q., Zhang, J., Du, M., Liu, Y., & Ji, G. (2012). Photodegradation of rhodamine B over unexcited semiconductor compounds of BiOCl and BiOBr. *Journal of Colloid Interface Science, 377*, 291–298.

Chen, Q. P., Li, J. H., Li, X. J., Huang, K., Zhou, B. X., Cai, W. M., & Shangguan, W. F. (2012). Visible-light responsive photocatalytic fuel cell based on WO_3/W photoanode and Cu_2O/Cu photocathode for simultaneous wastewater treatment and electricity generation. *Environmental Science & Technology, 46*(20), 11451–11458.

Choi, H., Shin, D., Yeo, B. C., Song, T., Han, S. S., Park, N., & Kim, S. (2016). Simultaneously controllable doping sites and the activity of a W-N codoped TiO_2 photocatalyst. *ACS Catalysis, 6*(5), 2745−2753.

Chowdhury, P., Athapaththu, S., Elkamel, A., & Ray, A. K. (2017). Visible-solar-light-driven photo-reduction and removal of cadmium ion with eosin Y-sensitized TiO_2 in aqueous solution of triethanolamine. *Separation and Purification Technology, 174*, 109−115.

Dahl, J. P., & Switendick, A. C. (1966). Energy bands in cuprous oxide. *Journal of Physics and Chemistry of Solids, 27*(6–7), 931–942.

Das, K., & De, S. K. (2009). Optical and photoconductivity studies of Cu_2O nanowires synthesized by solvothermal method. *Journal of Luminescence, 129*(9), 1015–1022.

El-Sheikh, S. M., Khedr, T. M., Hakki, A., Ismail, A. A., Badawy, W. A., & Bahnemann, D. W. (2017). Visible light activated carbon and co-doped mesoporous TiO_2 as efficient photocatalyst for degradation of ibuprofen. *Separation and Purification Technology, 173*, 258−268.

Feng, Y., Siow, K. S., Teo, W. K., Tan, K. L., & Hseih, A. K. (1997). Corrosion mechanisms and products of copper in aqueous solutions at various pH values. *Corrosion, 53*, 389–398.

Gao, Z., Liu, J., Xu, F., Wu, D., Wu, Z., & Jiang, K. (2012). One-pot synthesis of graphene-cuprous oxide composite with enhanced photocatalytic activity. *Solid State Science, 14*(2), 276–280.

Gonzalez, L. T., Leyva-Porras, C., Sanchez-Dominguez, M., Maza, I. J., & Rodriguez, F. E. L. (2017). Comparative photocatalytic performance on the degradation of 2-naphthol under simulated solar light using alpha-$Bi_4V_2O_{11}$ synthesized by solid-state and co-precipitation methods. *Water, Air, and Soil Pollution, 228*(2), 75.

Granbohm, H., Kulmala, K., Lyer, A., Ge, Y. L., & Hannula, S. P. (2017). Preparation and photocatalytic activity of quaternary GO/TiO_2/Ag/AgCl nanocomposites. *Water, Air, and Soil Pollution, 228*(4), –127.

Haldar, K. K., Sinha, G., Lahtinen, J., & Patra, A. (2012). Hybrid colloidal Au-CdSe pentapod heterostructures synthesis and their photocatalytic properties. *ACS Applied Materials & Interfaces, 4*(11), 6266–6274.

Huang, W.-C., Lyu, L.-M., Yang, Y.-C., & Huang, M. H. (2012). Synthesis of Cu_2O nanocrystals from cubic to rhombic dodecahedral structures and their comparative photocatalytic activity. *Journal of American Chemical Society, 134*(2), 1261−1267.

Huang, H. J., Zhang, J., Jiang, L., & Zang, Z. G. (2017a). Preparation of cubic Cu_2O nanoparticles wrapped by reduced graphene oxide for the efficient removal of rhodamine B. *Journal of Alloys and Compounds, 718*, 112−115.

Huang, Y., Yan, C. F., Guo, C. Q., Lu, Z. X., Shi, Y., & Wang, Z. D. (2017b). Synthesis of GO-modified Cu_2O nanosphere and the photocatalytic mechanism of water splitting for hydrogen production. *International Journal of Hydrogen Energy, 42*(7), 4007−4016.

Kecsenovity, E., Endrodi, B., Toth, P. S., Zou, Y., Dryfe, R. A. W., Rajeshwar, K., & Janaky, C. (2017). Enhanced photoelectrochemical performance of cuprous oxide/graphene nanohybrids. *Journal of American Chemical Society, 139*(19), 6682−6692.

Khurana, I., Saxena, A., Bharti, Khurana, J. M., & Rai, P. K. (2017). Removal of dyes using graphene-based composites: a review. *Water, Air, and Soil Pollution, 228*(5), 180.

Kumar, S., & Ojha, A. K. (2016). Ni, Co and Ni-Co codoping induced modification in shape, optical band gap and enhanced photocatalytic activity of CeO_2 nanostructures for photodegradation of methylene blue dye under visible light irradiation. *RSC Advance, 6*(11), 651–8660.

Kumar, S., Parlett, C., Isaacs, M. A., Jowett, D. V., Douthwaite, R. E., Cockett, M. C. R., & Lee, A. F. (2016). Facile synthesis of hierarchical Cu_2O nanocubes as visible light. *Applied Catalysis B Environmental, 189*, 226–232.

Kwon, Y., Soon, A., Han, H., & Lee, H. J. (2015). Shape effects of cuprous oxide particles on stability in water and

photocatalytic water splitting. *Journal of Materials Chemistry A, 3*(1), 156−162.

Landi, S., Carneiro, J. O., Fernandes, F., Parpot, P., Molina, J., Cases, F., Fernandez, J., Santos, J. G., Soares, G. M. B., Teixeira, V., & Samantilleke, A. P. (2017). Functionalization of cotton by RGO/TiO_2 to enhance photodegradation of rhodamine B under simulated solar irradiation. *Water, Air, and Soil Pollution, 228*(9), 335.

Leon, D. E., Zuniga-Benitez, H., Penuela, G. A., & Mansilla, H. D. (2017). Photocatalytic removal of the antibiotic cefotaxime on TiO_2 and ZnO suspensions under simulated sunlight radiation. *Water, Air, and Soil Pollution, 228*(9), 361.

Li, H. Q., Hong, W. S., Cui, Y. M., Hu, X. Y., Fang, S. H., & Zhu, L. (2014). Enhancement of the visible light photocatalytic activity of $Cu_2O/BiVO_4$ catalysts synthesized by ultrasonic dispersion method at room temperature. *Materials Science Engineering B, 181*, 1–8.

Li, F., Zhang, L., Tong, J. C., Liu, Y. L., Xu, S. G., Cao, Y., & Cao, S. K. (2016). Photocatalytic CO_2 conversion to methanol by Cu_2O/graphene/TNA heterostructure catalyst in a visible-light-driven dual-chamber reactor. *Nano Energy, 27*, 320−329.

Liu, S.-H., & Syu, H.-R. (2012). One-step fabrication of N-doped mesoporous TiO_2 nanoparticles by self-assembly for photocatalytic water splitting under visible light. *Applied. Energy, 100*, 148−154.

Liu, S.-H., & Syu, H.-R. (2013). High visible-light photocatalytic hydrogen evolution of C,N-codoped mesoporous TiO_2 nanoparticles prepared via an ionic-liquid template approach. *International Journal of Hydrogen Energy, 38*(32), 13856–13865.

Liu, G. G., He, F., Li, X. Q., Wang, S. H., Li, L. J., Zuo, G. F., Huang, Y., & Wan, Y. Z. (2011). Three dimensional cuprous oxide microtube lattices with high catalytic activity templated by bacterial cellulose nanofibers. *Journal of Materials Chemistry, 21*(29), 10637–10640.

Liu, S.-H., Syu, H.-R., & Wu, C.-Y. (2014). Alcohol solvents evaporation-induced self-assembly synthesis of mesoporous $TiO_{2-x-y}C_xN_y$ nanoparticles toward visible-light driven photocatalytic activity. *Journal of Nanoparticle Research, 16*(12), 2750.

Liu, S.-H., Wei, Y.-S., & Lu, J.-S. (2016a). Visible-light-driven photodegradation of sulfamethoxazole and methylene blue by Cu_2O/rGO photocatalysts. *Chemosphere, 154*, 118–123.

Liu, X. W., Shen, L. Y., & Hu, Y. H. (2016b). Preparation of TiO_2-graphene composite by a two-step solvothermal method and its adsorption-photocatalysis property. *Water, Air, and Soil Pollution, 227*(5), 141.

Mateo, D., Esteve-Adell, I., Albero, J., Primo, A., & Garcia, H. (2017). Oriented 2.0.0 Cu_2O nanoplatelets supported on few-layers graphene as efficient visible light photocatalyst for overall water splitting. *Applied Catalysis B Environmental, 201*, 582–590.

Mayorov, A. S., Gorbachev, R. V., Morozov, S. V., Britnell, L., Jalil, R., Ponomarenko, L. A., Blake, P., Novoselov, K. S., Watanabe, K., Taniguchi, T., & Giem, A. K. (2011). Micrometer-scale ballistic transport in encapsulated graphene at room temperature. *Nano Letters, 11*(6), 2396–2399.

Nadarajan, R., Abu Bakar, W. A. W., Ali, R., & Ismail, R. (2016). Effect of structural defects towards the performance of TiO_2/SnO_2/WO_3 photocatalyst in the degradation of 1,2-dichlorobenzene. *Journal of the Taiwan Institute of Chemical Engineers, 64*, 106−115.

Nalbandian, M. J., Greenstein, K. E., Shuai, D. M., Zhang, M. L., Choa, Y. H., Parkin, G. F., Myung, N. V., & Cwiertny, D. M. (2015). Tailored synthesis of photoactive TiO_2 nanofibers and Au/TiO_2 nanofiber composites: structure and reactivity optimization for water treatment applications. *Environmental Science & Technology, 49*(3), 1654−1663.

Nethravathi, C., & Rajamathi, M. (2008). Chemically modified graphene sheets produced by the solvothermal reduction of colloidal dispersions of graphite oxide. *Carbon, 46*(14), 1994–1998.

Niu, Z. G. (2014). Reduced graphene oxide-cuprous oxide hybrid nanopowders: hydrothermal synthesis and enhanced photocatalytic performance under visible light irradiation. *Materials Science in Semiconductor Processing, 23*, 78–84.

Ojha, D. P., Joshi, M. K., & Kim, H. J. (2017). Photo-fenton degradation of organic pollutants using a zinc oxide decorated iron oxide/reduced graphene oxide nanocomposite. *Ceramics International, 43(1*, 1290–1297.

Petronella, F., Truppi, A., Ingrosso, C., Placido, T., Striccoli, M., Curri, M. L., Agostiano, A., & Comparelli, R. (2017). Nanocomposite materials for photocatalytic degradation of pollutants. *Catalysis Today, 2017*(281), 85−100.

Pu, Y.-C., Chou, H.-Y., Kuo, W.-S., Wei, K.-H., & Hsu, Y.-J. (2017). Interfacial charge carrier dynamics of cuprous oxide-reduced graphene oxide (Cu_2O-rGO) nanoheterostructures and their related visible light-driven photocatalysis. *Applied Catalysis B Environmental, 204*, 21−32.

Reddy, P. A. K., Reddy, P. V. L., Kwon, E., Kim, K. H., Akter, T., & Kalagara, S. (2016). Recent advances in photocatalytic treatment of pollutants in aqueous media. *Environment International, 91*, 94–103.

Shang, Y., & Guo, L. (2015). Facet-controlled synthetic strategy of Cu_2O-based crystals for catalysis and sensing. *Advanced Science, 2*(10), 1500140.

Shen, B., Zhang, Y. H., An, Q., Yu, L., & Shang, J. W. (2015). Cu_2O immobilized on reduced graphene oxide for the photocatalytic treatment of red water produced from the manufacture of TNT. *Desalination and Water Treatment, 54*(2), 540−546.

Stankovich, S., Dikin, D. A. R., Piner, D., Kohlhaas, K. A., Kleinhammes, A., Jia, Y., Wu, Y., Nguyen, S. T., & Ruoff, R. S. (2007). Synthesis of graphene-based nanosheets via chemical reduction of exfoliated graphite oxide. *Carbon, 45*(7), 1558−1565.

Stoller, M. D., Park, S., Zhu, Y., An, J., & Ruoff, R. S. (2008). Graphene-based ultracapacitors. *Nano Letters, 8*(10), 3498–3502.

Su, F. Y., Xu, C. Q., Yu, Y. X., & Zhang, W. D. (2016). Carbon self-doping induced activation of n-pi* electronic transitions of g-C_3N_4 nanosheets for efficient photocatalytic H_2 evolution. *ChemCatChem, 8*(22), 3527−3535.

Sun, S. D. (2015). Recent advances in hybrid Cu_2O-based heterogeneous nanostructures. *Nanoscale, 7*(25), 10850–10882.

Tan, L. L., Ong, W. J., Chai, S. P., Goh, B. T., & Mohamed, A. R. (2015). Visible-light-active oxygen-rich TiO_2 decorated 2D graphene oxide with enhanced photocatalytic activity toward carbon dioxide reduction. *Applied Catalysis B Environmental, 179*, 160–170.

Tangale, N. P., Belhekar, A. A., Kale, K. B., & Awate, S. V. (2014). Enhanced mineralization of gaseous organic pollutant by photo-oxidation using Au-doped TiO_2/MCM-41. *Water, Air, and Soil Pollution, 225*(2), 1847.

Tao, S., Yang, M., Chen, H. H., Ren, M. Y., & Chen, G. W. (2017). Microfluidic synthesis of Ag@Cu_2O core-shell nanoparticles with enhanced photocatalytic activity. *Journal of Colloid Interface Science, 486*, 16−26.

Wang, W. Z., Wang, G. H., Wang, X. S., Zhan, Y. J., Liu, Y. K., & Zheng, C. L. (2002). Synthesis and characterization of Cu_2O nanowires by a novel reduction route. *Advanced Materials, 14*(1), 67−69.

Wang, M. Y., Huang, J. R., Tong, Z. W., Li, W. H., & Chen, J. (2013). Reduced graphene oxide-cuprous oxide composite via facial deposition for photocatalytic dye-degradation. *Journal of Alloys Compounds, 568*, 26–35.

Wang, J. T. W., Ball, J. M., Barea, E. M., Abate, A., Alexander-Webber, J. A., Huang, J., Saliba, M., Mora-Sero, I., Bisquert, J., Snaith, H. J., & Nicholas, R. J. (2014). Low-temperature processed electron collection layers of graphene/TiO_2 nanocomposites in thin film perovskite solar cells. *Nano Letters, 14*(2), 724–730.

Wu, T., Liu, G., Zhao, J., Hidaka, H., & Serpone, N. (1998). Photoassisted degradation of dye pollutants. V. Self-photosensitized oxidative transformation of rhodamine B under visible light irradiation in aqueous TiO_2 dispersions. *Journal of Physical Chemistry B, 102*(30), 5845–5851.

Xu, C., Cao, L. X., Su, G., Liu, W., Liu, H., Yu, Y. Q., & Qu, X. F. (2010). Preparation of ZnO/Cu_2O compound photocatalyst and application in treating organic dyes. *Journal of Hazardous Materials, 176*, 807–813.

Xu, L., Zhang, F. Y., Song, X. Y., Yin, Z. L., & Bu, Y. X. (2015). Construction of reduced graphene oxide-supported Ag-Cu_2O composites with hierarchical structures for enhanced photocatalytic activities and recyclability. *Journal of Materials Chemistry A, 3*, 5923−5933.

Yeo, B. E., Cho, Y. S., & Huh, Y. D. (2017). Evolution of the morphology of Cu_2O microcrystals: cube to 50-facet polyhedron through beveled cube and rhombicuboctahedron. *CrystEngComm, 19*(12), 1627–1632.

Yu, L. F., Zhang, S. M., Zhang, M., & Chen, J. D. (2017). Superhydrophobicity construction with dye-sensitised TiO_2 on fabric surface for both oil/water separation and water bulk contaminants purification. *Applied Surface Science, 425*, 46−55.

Zhang, J. L., Yang, H. J., Shen, G. X., Cheng, P., Zhang, J. Y., & Guo, S. W. (2010). Reduction of graphene oxide via L-ascorbic acid. *Chemical Communications, 46*(7), 1112−1114.

Zhang, W., Li, X. L., Yang, Z., Tang, X. M., Ma, Y. J., Li, M., Hu, N. T., Wei, H., & Zhang, Y. F. (2016a). In situ preparation of cubic Cu_2O-RGO nanocomposites for enhanced visible-light degradation of methyl orange. *Nanotechnology, 27*, 265703.

Zhang, Z. H., Zhai, S. Y., Wang, M. H., Ji, H. F., He, L. H., Ye, C. M., Wang, C. B., Fang, S. M., & Zhang, H. Z. (2016b). Photocatalytic degradation of rhodamine B by using a nanocomposite of cuprous oxide, three-dimensional reduced graphene oxide, and nanochitosan prepared via one-pot synthesis. *Journal of Alloys Compounds, 659*, 101–111.

Zhou, K. Q., Shi, Y. Q., Jiang, S. H., Hu, Y., & Gui, Z. (2013). Facile preparation of Cu_2O/carbon sphere heterostructure with high photocatalytic activity. *Materials Letters, 98*, 213–216.

Zou, W. X., Zhang, L., Liu, L. C., Wang, X. B., Sun, J. F., Wu, S. G., Deng, Y., Tang, C. J., Gao, F., & Dong, L. (2016). Engineering the Cu_2O-reduced graphene oxide interface to enhance photocatalytic degradation of organic pollutants under visible light. *Applied Catalysis B Environmental, 181*, 495−503.